




Cathodoluminescence studies of the optical properties of a zincblende InGaN/GaN single quantum well

Abhiram Gundimeda¹, Gunnar Kusch^{1,*}, Martin Frentrup¹, Menno J Kappers¹, David J Wallis^{1,2} and Rachel A Oliver¹

¹ Department of Materials Science and Metallurgy, University of Cambridge, 27 Charles Babbage Rd, Cambridge CB3 0FS, United Kingdom

² Centre for High Frequency Engineering, University of Cardiff, 5 The Parade, Newport Road, Cardiff CF24 3AA, United Kingdom

E-mail: gk419@cam.ac.uk

Received 13 October 2023, revised 4 January 2024

Accepted for publication 2 July 2024

Published 11 July 2024



Abstract

Zincblende GaN has the potential to improve the efficiency of green- and amber-emitting nitride light emitting diodes due to the absence of internal polarisation fields. However, high densities of stacking faults are found in current zincblende GaN structures. This study presents a cathodoluminescence spectroscopy investigation into the low-temperature optical behaviour of a zincblende GaN/InGaN single quantum well structure. In panchromatic cathodoluminescence maps, stacking faults are observed as dark stripes, and are associated with non-radiative recombination centres. Furthermore, power dependent studies were performed to address whether the zincblende single quantum well exhibited a reduction in emission efficiency at higher carrier densities—the phenomenon known as efficiency droop. The single quantum well structure was observed to exhibit droop, and regions with high densities of stacking faults were seen to exacerbate this phenomenon. Overall, this study suggests that achieving efficient emission from zinc-blende GaN/InGaN quantum wells will require reduction in the stacking fault density.

Supplementary material for this article is available [online](#)

Keywords: zincblende, cathodoluminescence, quantum well, stacking faults, droop

1. Introduction

III-nitride material systems have been extensively used for various optoelectronic applications, mainly light emitting diodes (LEDs) [1–3]. Conventional white light LEDs are made by utilising blue LEDs based on wurtzite (wz) InGaN/GaN

multi-quantum wells (MQWs) with a phosphor cap, which absorbs some of the blue light and emits longer wavelength light [4]. This inevitably leads to energy losses [5, 6]. An alternative to this down-conversion using phosphor materials is colour mixing of separate blue, green, and red LEDs. Of these LEDs, commercial wz-GaN-based blue and InGaAsP-based red LEDs are very efficient. However, the efficiency of wz-GaN-based green LEDs is nearly half that of red and blue LEDs, known as the ‘green gap’ problem [7], and is related to inherent limitations of wz-GaN based LEDs. In wz-GaN based LEDs grown in the (0001) orientation, spontaneous and piezoelectric polarization fields are present, causing a strong quantum confined Stark effect (QCSE). These fields reduce the

* Author to whom any correspondence should be addressed.



Original content from this work may be used under the terms of the [Creative Commons Attribution 4.0 licence](#). Any further distribution of this work must maintain attribution to the author(s) and the title of the work, journal citation and DOI.

electron-hole wavefunction overlap, resulting in a reduction of the rate of radiative recombination and thus making it less competitive with non-radiative processes [8]. This causes a decrease in the internal quantum efficiency (IQE) of the LEDs.

Additionally, to reach green emission, either more indium needs to be incorporated into the InGaN/GaN QWs or the QW thickness needs to be increased, in comparison to blue light emitting QWs. This increase in the InN content in the QWs is typically achieved by growing the heterostructure at a lower temperature, which has been suggested to lead to incorporation of a higher density of point defects and can possibly increase the inhomogeneity of the InN composition in the QWs [9–11]. Such point defects may act as non-radiative recombination centres, while any inhomogeneity of the InGaN QWs can lead to poor spectral purity of wz-based InGaN/GaN QWs [12–14].

Cubic zincblende (zb) GaN is a metastable phase of GaN, which in comparison, should not exhibit such inherent polarization fields when grown in the (001) orientation and has a lower bandgap than wz-GaN. In consequence, it is expected that a lower proportion of InN will be required to achieve green emission [15]. Such advantages should in theory allow for a much higher IQE in long wavelength devices. Despite these advantageous properties, current zb-InGaN/GaN QW based LEDs are still lacking in efficiency. One reason for this may be the presence of high defect densities, in particular {111}-type stacking faults (SFs) and wz inclusions [16, 17]. While high phase purities with low or no wz inclusions can be achieved by optimizing the growth conditions [17–19], SFs are formed right at the beginning of the heteroepitaxial growth at an angle of about 55° with respect to the (001) growth plane. As they are also inclined with respect to each other these SFs reduce in density with increasing film thickness by defect reactions, but they might not be completely avoidable [16] and hence some of the SFs might reach and intersect the QWs. Despite the theoretical advantages of zb-GaN over wz-GaN, it is thus still necessary to develop a good understanding of the effect of SFs on the optical properties of zb-InGaN-based QWs. An insight into how these SFs behave optically is essential as they may hamper the overall light emission quality of LEDs based on zb-QWs.

Very few reports are present in the literature that study the optical behaviour of SFs in zb-GaN [20–23]. Kemper *et al* performed cathodoluminescence (CL) spectroscopy studies in the scanning transmission electron microscope (STEM) to assess the influence of SFs on the optical emission in zb-GaN epilayers and demonstrated that SFs lead to a reduced CL emission intensity [20]. Lorenz *et al* [21] and Wei *et al* [22] highlighted that the presence of these SFs can lead to the formation of wz inclusions in the epilayers. This significantly affects the optical quality, as any optical emissions from the wz phase leads to poor spectral purity in zb-InGaN/GaN QWs, i.e. a shift and broadening in emission energies. Besides formation of wz inclusions, or {111}-type SFs running through the QWs can also alter the local distribution of Indium [23, 24].

Ding *et al* performed multi-microscopy studies on a cross-sectional TEM lamella of a zb-GaN LED heterostructure with SFs running through the QWs [23]. In regions where SFs were observed running through the QWs indium segregation next to the SFs in the InGaN QWs was seen. The presence of this phenomenon led to inhomogeneous emissions throughout the QWs with regions where SFs interact with the QW exhibiting lower energy CL emission than the main QW.

Current blue LEDs, made of wz-GaN, have a high peak radiant efficiency of >80% [25]. However, as the injection current density increases, the light output efficiency of wz-GaN LEDs decreases [26]. This phenomenon is known as efficiency droop or droop for short. Applications such as general lighting require high brightness, which indicates that the used LEDs need to emit a high flux of photons. If we utilise smaller devices, large currents need to flow through the devices, which leads to a drop in efficiency. One can use multiple devices at low currents or larger devices at low currents, but this becomes expensive. It is essential to achieve high brightness and high efficiency while keeping the costs down. Additional applications such as micro-displays, which intrinsically require small device sizes, also lead to high current densities leading to inefficient devices. Extensive research has been carried out in understanding the carrier mechanisms that triggers the droop mechanism in wz-based InGaN/GaN QWs [26]. However, only sparse information can be found in the literature regarding droop in zb-InGaN QWs. Tsai *et al* simulated the optical behaviour of zb-InGaN based LED structures and wz-InGaN based LED structures including their dependence on the current density [27]. Both structures had identical design parameters such as p and n doping concentrations, QW thickness and InGaN composition. In the simulations both devices displayed the droop phenomenon, but it was much more pronounced in the wz device. The enhancement of the droop phenomenon in the wz structure was attributed to the presence of polarisation fields and a large carrier mass. These polarisation fields are absent in zb-GaN when grown in the (001) orientation and the carrier effective mass is lower in zb-GaN, which reduced the droop in zb-GaN theoretically by 51%. These simulations provide a hint that the droop phenomenon in zb-GaN material may be less of an issue than in wz-InGaN LED structures.

In this study, we use CL spectroscopy to investigate the optical properties of a zb-InGaN/GaN single QW (SQW) structure. In particular, the impact of SFs on light emission from a single InGaN QW is studied. Furthermore, to investigate whether the SQW structure suffers from droop, a detailed CL study with varying beam current was carried out while keeping the interaction volume constant.

2. Experimental details

The zb-InGaN/GaN SQW heterostructure studied in this work was grown on a 3C-SiC/Si (001) substrate in a 6 × 2' Aixtron

close-coupled showerhead metal organic vapour phase epitaxy reactor. The substrate consists of a 3.5 μm thick layer of (001) oriented 3C-SiC grown on a 750 μm thick Si wafer with a 4° miscut towards the [110] in-plane direction. The substrate miscut was introduced to avoid the formation of antiphase domains [16]. First, a 30 nm thick GaN nucleation layer and an approximately 800 nm thick zb-GaN buffer layer were grown, followed by a 40 nm thick InGaN underlayer, with an InN composition of 1%–2%. On top of the InGaN underlayer a SQW with a thickness of about 2 nm and a targeted composition of about 10% InN (i.e. $\text{In}_{0.1}\text{Ga}_{0.9}\text{N}$ QW) was grown. The SQW was then capped with an 8 nm thick GaN barrier layer. The other growth parameters used for the growth of the SQW are similar to the conditions typically used for *c*-plane wurtzite InGaN QWs [28]. A schematic diagram representing the zb-InGaN/GaN SQW structure is shown in the supplementary information (figure S1).

Hyperspectral CL measurements along with secondary electron (SE) imaging were performed using an Allalin 4027 Chronos scanning electron microscopy CL system with a 150 l/mm grating (blazed at 500 nm). All measurements were performed at an excitation voltage of 3 kV and a temperature of 10 K, maintained using a liquid Helium cryostat in order to limit the diffusion length. The beam current was varied from 63 pA to 30 nA as measured by a Faraday Cup. Monte Carlo simulations with the software Casino [29] revealed that under these conditions the incident electrons lose 90% of their energy at a depth of about 47 nm from the sample surface, which covers the SQW and some part of the InGaN underlayer.

3. Results and discussion

As the surface morphology can give a first important insight into the morphology of the SQW buried underneath the surface, SE images were collected of the sample. Figure 1(a) shows the SE image of the zb-InGaN/GaN single quantum well structure. Overall, several elongated surface features along with flat regions are distributed across the surface. The elongated features are observed to be aligned both perpendicular and parallel to the miscut direction, i.e. in both the [1–10] direction and the [110] direction, marked by arrow-1 and arrow-2 in figure 1(a), respectively. Furthermore, pale stripes are observed on the surface, parallel to the [110] miscut direction, marked by arrow-3 in figure 1(a). These are notably different from the other elongated features observed on the surface, as they have relatively less contrast, indicating a smaller local height or composition variation. The white box indicates a region where little to no surface features are present. The small bright dot features present on the surface, in figure 1(a), can be attributed to contamination.

To investigate the variation in optical emission in the InGaN/GaN SQW sample the panchromatic CL intensity map in figure 1(b) has been recorded on the same area shown in the SE image (figure 1(a)). In the panchromatic CL image, large, isolated, regions of high emission intensity can be observed on the surface. An example is marked by the white box in figure 1(b). These regions are adjacent to areas with

very low emission intensity. Also, we can observe stripes of high CL intensity running parallel to the miscut direction, along [110]. These stripes are interrupted by regions of low CL intensity, indicating the presence of non-radiative recombination centres. Non-radiative recombination can occur at point defects, threading dislocations or SFs [20, 30–37]. Even though there are dark regions in the image, these are not regions of zero emission but of relatively low emission intensity compared to the surrounding material.

Correlating the SE image with the panchromatic CL image gives an insight into the variation in CL emission intensity with respect to the morphology. The high intensity regions present in the panchromatic CL map (white box in figure 1(b)) correlate with a flat surface region in the SE image (white box in figure 1(a)) which is free from elongated surface features. Such flat high intensity regions are also observed at the bottom of the SE image (figure 1(a)) and the panchromatic CL map (figure 1(b)). The features running parallel (along [110]), and perpendicular (along [1–10]) to the miscut direction (marked by arrow 1 and 2 respectively in figures 1(a) and (b)) have very different optical properties. We attribute this to the structure of the region surrounding either of these features. The features perpendicular to the miscut direction, are surrounded by flat regions free from any pale stripes, whereas the features parallel to the miscut direction are surrounded by single or multiple pale stripes. The pale stripes observed in the SE image (marked by arrow-3 in figure 1(a)) themselves exhibit low CL emission intensity (marked by arrow-3 in figure 1(b)), which indicates that they are areas of high non-radiative recombination.

The overall mean CL spectrum of the imaged area in the SQW sample is shown in figure 1(c). It reveals an emission peak centred at 3.00 eV with a FWHM of 260 meV. This peak is associated with emission originating from recombination in the InGaN/GaN SQW. A broad low-energy shoulder peak was observed, which can be associated with a strong inhomogeneity of the emissive layer across the sample. This can include variations of the QW as well as other luminescence centres which will be discussed in detail later.

Comparing the spot spectra, obtained from the hyperspectral CL map, at the different surface features observed in the SE image gives an insight into the CL emission energies of these features, as shown in figure 1(d). The high intensity flat region (white box in figure 1(a)) exhibits a peak emission energy at 3.00 eV. We observe a red shift in peak emission energy of ~ 190 meV for all investigated features perpendicular to the miscut direction (arrow-1 in figure 1(a)) along with a drop in the absolute peak intensity by 50%, in comparison to the high intensity regions (white box in figure 1(b)). A high energy shoulder can be observed for this spectrum whose energy matches the main QW emission from the flat region. The peak emission energy of the features parallel to the miscut direction, (arrow-2 in figure 1(a)) is about the same as for the elongated feature perpendicular to the miscut direction. However, the peak intensity in these regions drops by two orders of magnitude compared to the mean emission intensity obtained from the area in the white box in figure 1(b). It is evident from these spot spectra that the mean spectrum is dominated by the bright flat areas.

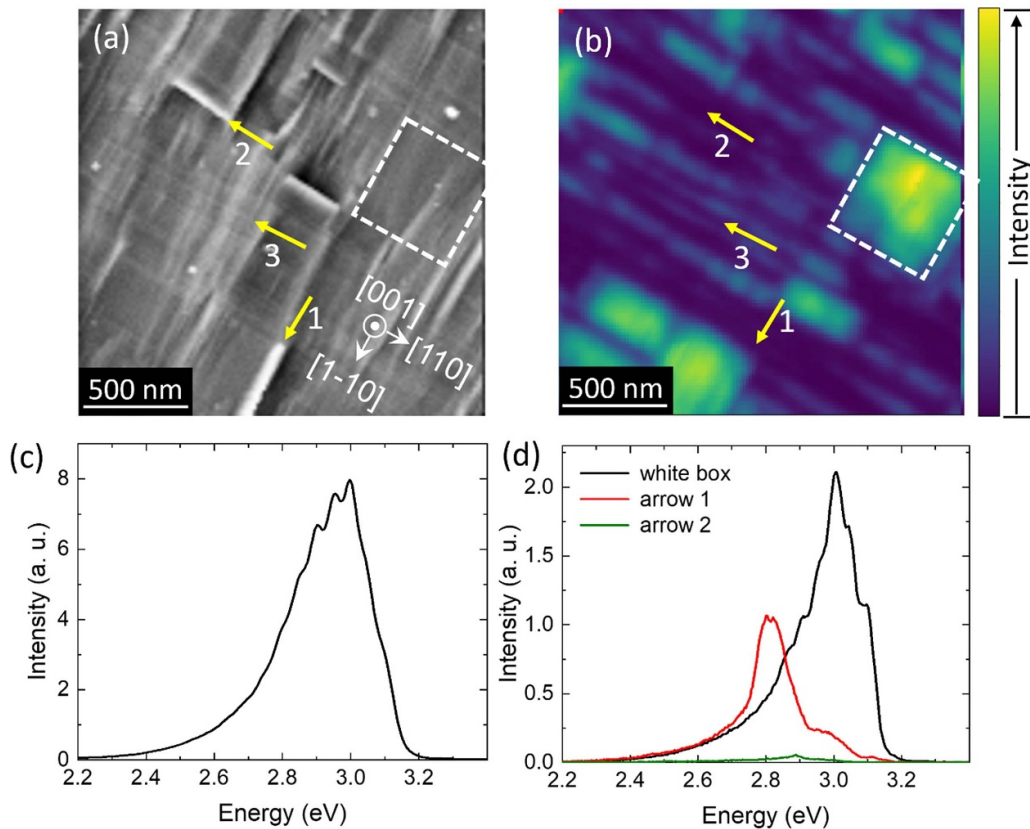


Figure 1. (a) Representative planar SE image, (b) low temperature (10 K) panchromatic CL intensity map of the zb-InGaN/GaN single quantum well structure. The white dashed box indicates a flat region, arrow 1 indicates a surface feature along [1-10], arrow 2 indicates a surface feature along [110] and arrow 3 indicates a pale stripe. (c) Mean spectrum (averaged over the mapped area) of the whole imaged region and (d) comparison between spectra from single pixels (arrow 1 and 3) and averaged emission from area within the white box.

In the initial analysis of the SE image (figure 1(a)), we identified pale stripes running across the surface of the SQW sample and found that they are corresponding to regions of significantly reduced CL emission intensity (figure 1(b)). A closer look at these regions was performed to isolate regions with pale single stripes and also bunches of stripes and assess their impact on light emission. For this, a region with clear pale stripes running across the surface, as shown in figure 2, was chosen. Some of these stripes are marked by yellow dotted lines (i–iv) in the SE image, figure 2(b), highlighting that they are aligned parallel to the miscut direction. The spacing between these pale stripes appear quite random; in some regions single or only a few stripes run across the surface, while there are also regions with bunches of pale stripes present. Two isolated pale stripes, marked i and ii, run parallel to each other. Both regions appear dark in the panchromatic CL image in figure 2(c) and the regions between them appear bright. This indicates that these pale stripes are rich in non-radiative recombination centres. Similar pale stripes are labelled as iii and iv in figures 2(a) and (b). The region between these stripes, marked by the yellow arrow 2, exhibits high CL intensity, whereas the region with a high density of these pale stripes, marked by arrow 1, shows extremely low

light emission with a measured drop in intensity by two orders of magnitude.

The presence of these non-radiative recombination centres in the InGaN/GaN structures could be attributed to several possible factors like point defects [38], line defects such as misfit dislocations or threading dislocations [37] and/or planar defects such as SFs [20]. Taking a closer look at these regions of low emission from the CL image in figure 2, one can see that the region is a pale stripe-like structure rather than being spotty. Spottiness would be typical for point defect clusters or point defects [38, 39]. There may be a possibility that if the defect density is high enough, they would not appear spotty-like, but the individual spots would merge and may form lines. However, it would be difficult to explain why there would be a preferential incorporation of point defects along a well-defined line without the presence of other defects. Another option for the observation is the presence of 1D defects. Misfit dislocations can, in principle, form to accommodate the lattice mismatch between the SQW and the surrounding material. However, a detailed high-resolution STEM study by Ding *et al* on similar zb-InGaN/GaN MQWs found no misfit dislocations newly formed in the MQWs [23]. If such misfit dislocations do not form in MQWs, they are even less likely to

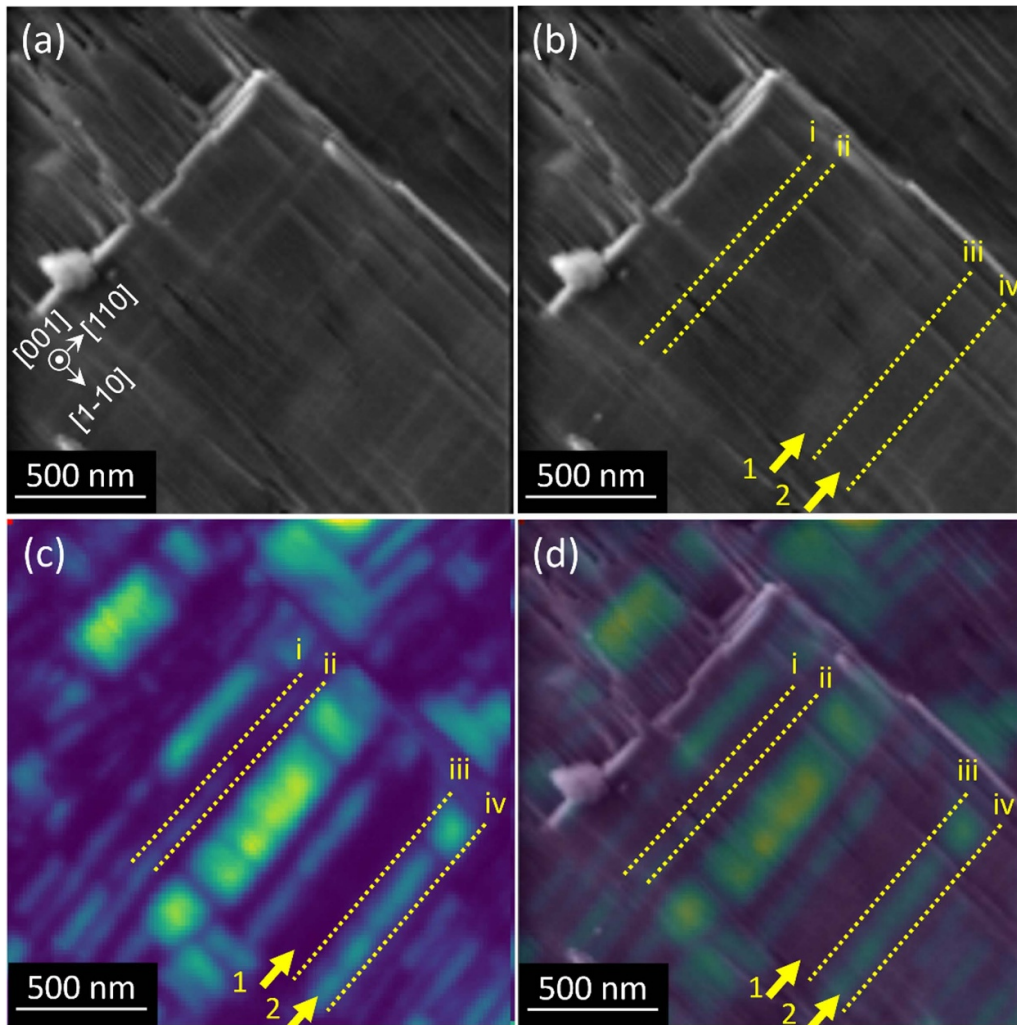


Figure 2. SE image of InGaN/GaN SQW sample (a) without and (b) with yellow lines matching with pale stripes and their corresponding (c) panchromatic CL image. (d) An overlay of the SE image and the panchromatic CL intensity image along with SF identification lines highlighting the non-radiative nature of the SFs. The yellow arrows indicate the regions of pale stripes marked by 1 and a region without SFs marked by 2.

form in a SQW, because the accumulated strain energy is smaller for a single layer, providing a weaker driving force for dislocations to form. This does not completely rule out misfit dislocations as the origin for the non-radiative areas in the CL map. However, given that Ding *et al* report of a high density of $\{111\}$ SFs from the epilayer crossing the QWs [23] and given that a high density of dark regions in the panchromatic CL maps are observed, it is much more likely that SFs are the relevant defect here.

As discussed earlier, in the panchromatic CL images the regions associated with the pale stripes in the SE images appear dark. This can be explained by the optical properties of SFs in zb-GaN, which are significantly different from SFs in wz-GaN [31, 36, 40]. As a simplified picture, one can consider a SF in wz-GaN as a monolayer-wide zb insertion and vice versa. At low temperatures, the zb SFs in wz-GaN are optically active and bright. The band gap of zb-GaN is smaller than that of wz-GaN, and these SFs in wz-GaN act as a QW thereby confining the electron and hole together in a

reduced volume [36, 41]. This increases the probability of recombination, giving brighter emission. In contrast, at room temperature these SFs in wz-GaN have reduced intensity [42]. This has been attributed to several factors in the literature, but the most common suggestion is the presence of point defects and dislocations at or around a SF that led to non-radiative recombination pathways [20, 43, 44]. As the carriers need little energy to escape the QW formed by the SF, and at room temperature thermal energy is available, carrier can diffuse to these low energy defect sites thereby leading to non-radiative recombination.

In the case of zb-GaN, a SF is a wz insertion, which has a wider band gap than the surrounding zb-GaN. Electron-hole pairs generated in the SFs can diffuse into the surrounding zb-GaN material where they could recombine radiatively, which would lead to emission intensity similar to the surrounding material. However, we observe dark stripes in the panchromatic CL maps, which implies that there must be non-radiative recombination associated with the SF or its

immediate surroundings. This is also supported by the work from Kemper *et al* [20] who observed, in cross-sectional TEM-CL maps of zb AlN/GaN MQWs, that regions around SFs exhibit low CL intensity, whereas regions in the zb material free from these defects produce higher intensity light emission. Based on all these findings we conclude that the pale stripes that are observed in this work are identifiable as individual SFs and/or SF bunches, acting as non-radiative recombination centres, either due to their inherent nature or due to decoration with point defects. Furthermore, we note that these pale stripes tend to locally lie mostly along the same orientation (similar to arrow-3 in figure 1(a)) along [110]. Additionally, we also observe a lower density of pale stripes along [1–10] direction. This is consistent with previous study which shows an anisotropy of SF orientation in similar samples [16]. SFs typically form on {111} planes at a specific angle to the GaN/SiC interface. The anisotropy in SFs can result from introducing a miscut into SiC/Si substrates to address anti-phase domains. This contributes to the creation of step bunches with {111} microfacets, favouring the formation of SFs.

We note that in the above discussion we address the carrier dynamics at SFs based on the relative bandgaps of the zb and wz material. However, the band alignments between the two materials may also play an important role. Unfortunately, even for GaN, there is some ambiguity in the literature as to whether the band alignment is type I [31, 45–47] or type II [48–50]. To fully understand the carrier dynamics here, we would need to know the band alignments between zb and wz materials in strained InGa_N, a point which has received almost no attention in the literature. This issue requires further study, if the impact of defects in either non-polar wz–InGa_N QWs or zb–InGa_N QWs is to be fully understood.

3.1. Droop in zb–GaN

As highlighted in the introduction, droop is an important phenomenon that can occur in an LED device, thereby hampering the overall light output from the device. We have also demonstrated in the previous section, that SFs are associated with non-radiative recombination. SFs running through the QWs can lead to local indium agglomeration as shown by Ding *et al* [24], which is expected to result in linewidth broadening [24]. Hence, they have a deleterious effect on the QW performance. By performing beam current dependent CL measurements, we can separate the impact of changing the carrier density on regions with and without SFs (which we identified in the previous section), thereby trying to address the impact of SFs on droop.

Initially, we conducted current-dependent studies by repeatedly exposing one region to varying beam currents, ranging from low to high (see supplementary information figure S2). Upon re-measuring the same region at lower currents, we observed a drop in intensity compared to the initial intensity level. This highlighted that the electron beam can damage the zb InGa_N QW, making it challenging to distinguish between the effects of beam damage and the droop phenomenon at high currents. To mitigate this issue, current-dependent studies were performed on different regions to

minimise beam damage at higher currents. To mitigate this issue, current-dependent studies were performed on different regions to minimise beam damage at higher currents. For this purpose, areas across the sample surface with similar surface morphology have been selected. To have consistent data at one beam current for comparison and normalization, panchromatic maps were obtained at the lowest current (63 pA) for all the areas. Then measurements with one more beam current (either 250 pA, 1, 3, 5, 10, 20, or 30 nA) have been performed at each area. Furthermore, all measurements were performed at low temperature (10 K) to limit the diffusion length. Figure 3 gives an overview of selected regions with significant change in the CL maps (here 250 pA, 3, and 30 nA). The SE images (left column) show the same general morphology that we have previously discussed, with protruding surface features and SFs present in the imaged areas. The initial CL measurements performed at 63 pA for each region are shown in figure 3 (middle column). These panchromatic CL images reveal, similar to the observations in the previous section, high emission intensity blocks as well as stripes of lower emission intensity.

After the initial measurements at 63 pA, CL imaging was performed at higher beam currents (figure 3, right column). For the CL measurement at 250 pA, the CL intensity variation of the surface remained similar to that of the region measured at 63 pA with high intensity emission in rectangular blocks and the presence of stripes parallel to the [110] miscut direction. The small spatial offset observed between the 63 and 250 pA panchromatic images is attributed to microscope drift. Overall, the average absolute intensity of the bright rectangular blocks increased with increasing current. A further increase in current to 1 and 3 nA, revealed small to no variations in the optical properties (not shown).

At 5 nA, the high intensity blocks act similarly to those previously observed, where the centre of the block retains high emission intensity. However, the emission of the edges of these blocks seems to drop in relative intensity and sharpness (evident in figure 3) compared to the centre of the blocks, potentially indicating an increase in the carrier diffusion length. Furthermore, we can see that the low intensity stripes have disappeared from the image. This may be attributable to a relative increase in the intensity of the blocks, which leaves the emission obtained from the stripe regions unobservable due to the colour scale chosen here. While the absolute intensity of these stripes is increasing with respect to other currents, they do not increase at the same rate as the SF free blocks. The same observation was made for measurements at 10 and 20 nA where the overall absolute intensity of pale stripes and SF free regions is increasing but the increase in intensity is slower in stripe like regions than in SF free regions. At 30 nA, the high intensity blocks associated with flat regions are the only features clearly visible in the panchromatic CL maps. The stripe like regions have much lower CL emission intensity, such that they cannot be observed at all in the linearly scaled intensity plots.

A comparison of the mean spectra across all regions is shown in figure 4(a). For this plot, all spectra have been normalised to the mean spectrum peak intensity of the 63 pA spectrum measured at the same area. At 250 pA, the mean spectrum has a peak emission energy at 2.95 eV with a FWHM of

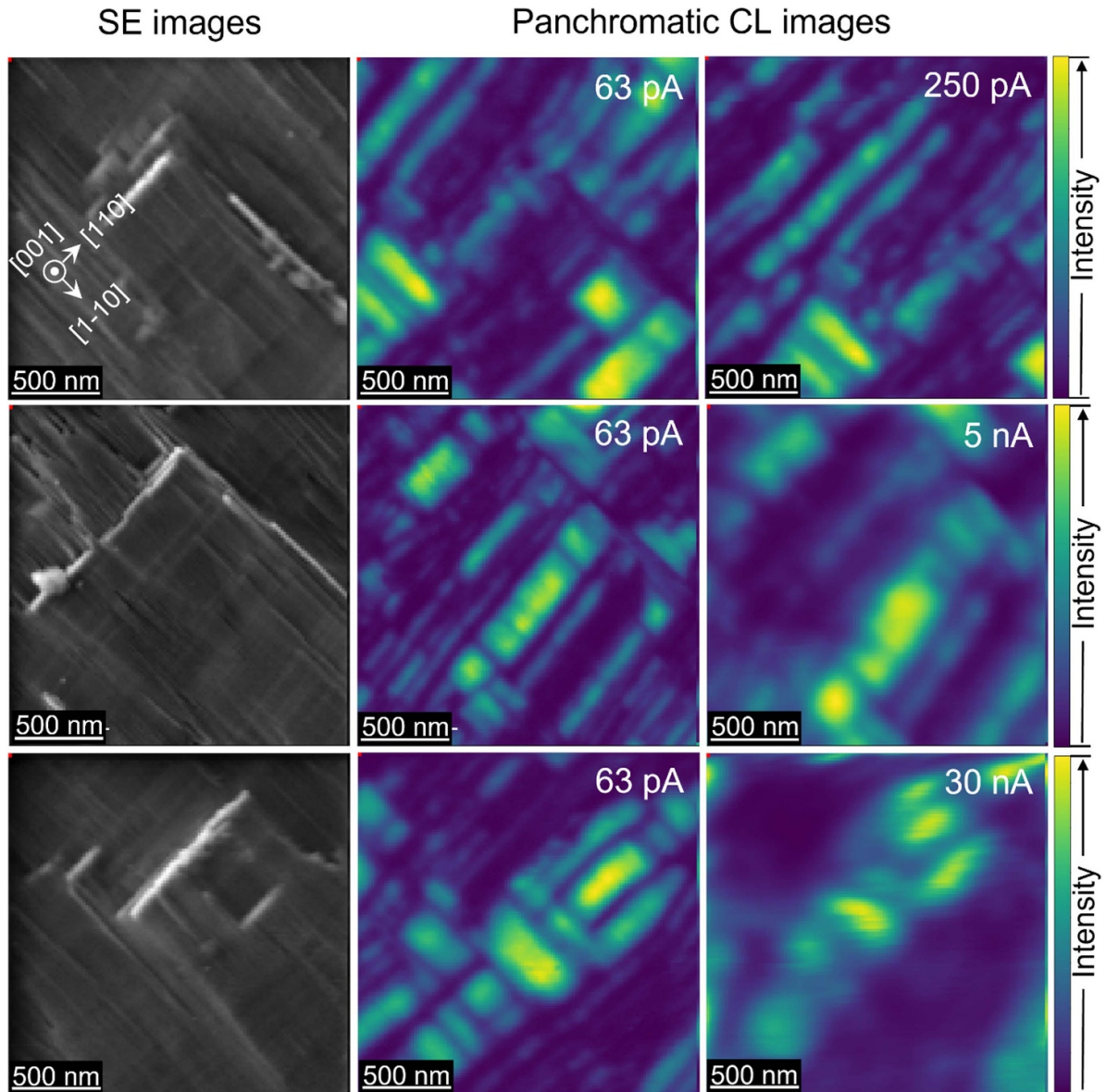


Figure 3. SE images of the InGaN/GaN SQW sample measured across different areas and a comparison between the panchromatic CL images measured at 63 pA and at varying beam currents between 250 pA and 30 nA.

210 meV. With increasing current, the peak intensity gradually increases. A small red shift in the peak position of 5 meV with increasing currents from 1 to 3 nA followed by a small blue shift by 5 meV when increasing currents from 3 to 5 nA can be observed. Such a shift is likely to relate to slight inhomogeneities in indium incorporation over the surface as the spectra are measured at different regions. Therefore, we concluded that within the accuracy of our measurements the overall main emission energy is independent of the current about (2.95 ± 0.005) eV. This indicates that there is no blue shift in emission energies with increasing current as is typically observed for conventional *c*-plane wz QWs [51]. Such a blue shift is observed for wz QWs because of the screening of the polarisation fields with increasing carrier density, leading to a reduction in the QCSE. The absence of such a blue-shift in the investigated zb-GaN SQW is evidence of the zb-GaN

SQW being free from polarisation fields as theoretically predicted. We note that we also do not observe any impact of state filling with increased current density in these samples.

Figure 4(b) shows the integrated intensities of the mean spectra as a function of the applied beam current. With increasing current, a sublinear increase in intensity similar to a square root function indicated by the dashed guide-to-the-eye line was observed. Only the data point at a current of 20 nA deviates from this trend, but we believe that this may be an outlier. Such an outlier is likely given the methodology, which involved taking each measurement on separate regions, so that spatial inhomogeneities in the sample will impact the data set. We treat the circled data point at 20 nA (figure 4(b)) as the anomaly rather than the data point at 30 nA because in the alternative case a smooth trend line would deviate from the data certainly at 10 nA and probably also at 5 nA. Overall, figure 4(b)

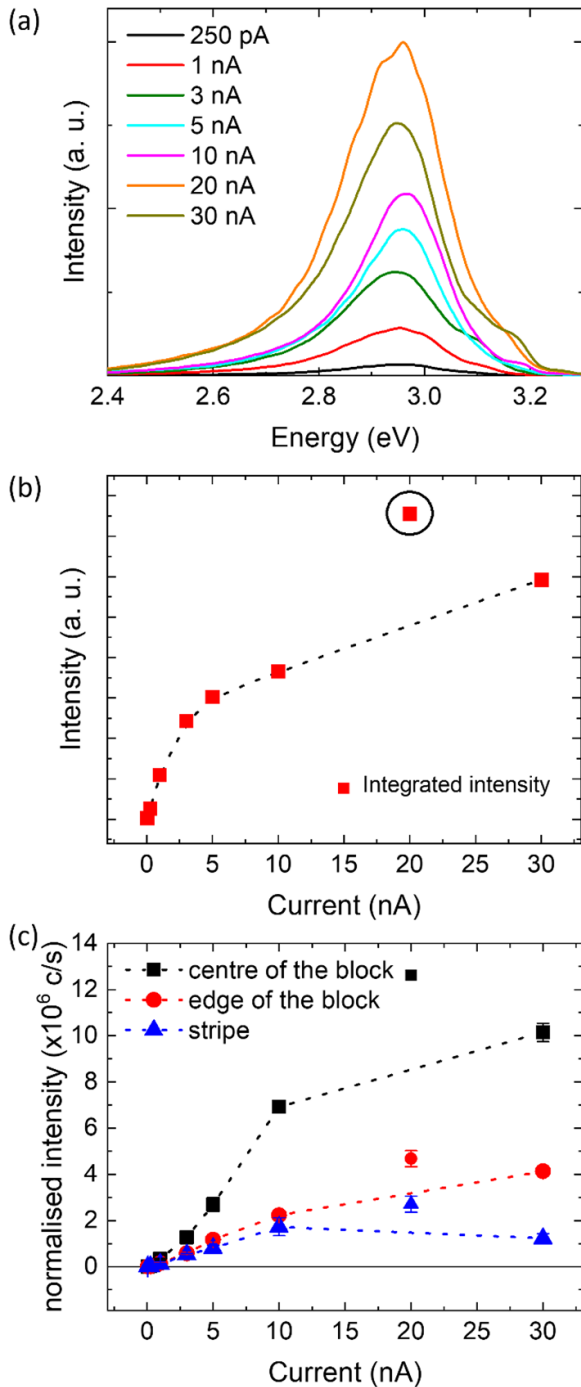


Figure 4. (a) Mean spectra of different areas of the InGaN/GaN SQW measured with different beam currents. All intensities are normalised to the 63 pA mean spectrum intensity of the corresponding area. (b) Calculated integrated intensities of the mean spectrum across each area with varying beam currents. The black circle indicates a circled data point which is considered as an outlier. (c) Graph showing the variation of the integrated intensity of emission, normalised to the emission from the same region at 63 pA for equal-sized regions at the centre of the high intensity blocks, the edges of the high intensity blocks and the stripey regions. In (b) and (c), the dotted lines are a guide to the eye. The error bars show standard deviation across the investigated data points.

implies that this SQW exhibits the droop phenomenon, which is generally characterised by a sub-linear increase in emission intensity with current density.

Possible non-radiative recombination loss processes which lead to efficiency droop have been discussed in the context of hexagonal wz-GaN-based MQW structures [26]. Among them are the Auger–Meitner recombination and carrier delocalisation, which both become more relevant at high currents [26]. It is expected that the same processes may be relevant in zb-GaN based QW structures. However, theoretical simulations predict a significantly smaller droop in the case of zb-GaN compared to hexagonal wz-based QW structures [27]. This was attributed to better electron-hole wavefunctions overlap in comparison to wz-GaN which leads to faster radiative recombination, reducing the carrier density at an equivalent current density. However, these simulations always consider crystalline perfect defect-free material and do not consider the rich defect structure in real zb-GaN material.

To study the role of such defects—predominantly SFs—in the observed droop in zb-GaN based SQW, individual regions in the hyperspectral CL maps have been studied in more detail. By comparing the CL maps in figure 3, it is evident that different features have varied intensity with respect to increasing currents. At all currents, we observe the flat regions which seem free from SFs remaining bright relative to the surrounding material. However, the edges of these flat regions (close to surrounding SFs) and the bright stripes (separated by adjacent SFs) in the CL maps do not maintain their brightness relative to these bright stripes as the current density increases. To quantify this, we plot figure 4(c), which shows the variations in intensity with increasing current for three different types of regions: the centre of the high intensity blocks, the edges of the high intensity blocks, and the stripey regions (figure S3 in the supplementary information). For each type or region, four measurements have been made, and the data come from areas of equal size. All intensities are normalised to the intensity at 63 pA for the relevant area.

For currents up to 20 nA, the graph in figure 4(c) shows the same trend that we have observed by eye: the emission from the edges of the high intensity blocks and the stripey regions increases in intensity as the measurement current increases, but the rate of increase is slower relative to the centre of the high intensity block. Also, the data for the centre of the high intensity blocks strongly resemble the data in figure 4(b) from the mean spectra, showing that these regions dominate the total emission. All the different regions show a sub-linear increase in intensity with measurement current. This is most pronounced at the highest measurement current. Given that the data points taken at 20 nA are suggested to come from an anomalously bright region, as explained above, the fact that for all three types of regions we see a drop in intensity from 20 to 30 nA is likely an artefact of the measurement approach. However, for the stripey regions, the emission intensity at 30 nA is slightly lower than the emission intensity at 10 nA. This

may indicate that we are not purely measuring droop phenomena here, but that we are observing damage to the sample. We know that the electron beam may damage these samples, as is evidence in the supplementary information (figure S2). It is possible that the stripey regions—where SFs are present—are more vulnerable to damage—than regions with less defects. This might be because there is indium segregation adjacent to the SFs and high indium content material may be more damage-prone. Alternatively, it might relate to distortion of bonds in the faulted region again leading to a greater vulnerability to damage.

However, within all these caveats, the data in figure 3 taken together may hint at the possibility that the presence of SFs—whether in the stripey regions or bounding the high intensity blocks—may exacerbate the droop phenomena in zb-InGaN QWs. This seems a reasonable suggestion, given that we have shown elsewhere using TEM that Indium segregates adjacent to the SFs [24]. This could lead to locally higher carrier densities in the segregated regions than in the SF-free regions, so that droop via the Auger–Meitner effect is exaggerated in the highly defected regions. An alternative explanation might be that at these highest currents available localised states related to well width or compositional fluctuations fill up [52]. Carriers can then access a continuum of states and can diffuse over longer distances. If the SF in and of itself acts as a non-radiative centre at high carrier densities, it may be that diffusion via this continuum of states at the highest carrier densities allows carriers from the local region to access the SF and recombine non-radiatively. However, even if the SF itself is not a non-radiative centre, it still represents a wz inclusion in a zb matrix, and the work of Ding *et al* [24] suggest that In segregates adjacent to the SF rather than on the SF. Both these points suggest that the SF itself will have a higher local bandgap than the surrounding material and thus present a barrier to carrier diffusion. Hence, carriers may diffuse parallel to the SF to threading dislocations or other defects which act as SF terminations, and there recombine non-radiatively.

4. Conclusion

In conclusion, a detailed investigation of the low-temperature optical behaviour of a zb-GaN/InGaN SQW LED structure is presented. The SQW structure revealed non-uniform distribution of emission intensity and emission energy. Regions with pale stripes in SE image were identified as individual SFs or SF bunches, which are associated with non-radiative recombination centres and lead to reduced intensity of light emission. This is either due to their inherent nature or due to decoration with point defects.

Power dependent studies were performed to investigate the droop behaviour of the SQW structure in general and the influence of SFs in particular. Overall, the SQW structure itself did suffer from the droop phenomenon. These measurements also gave proof of absence of polarization fields in the zb-GaN QWs since no significant shift in emission peak energy was seen with varying current densities. Additionally, we suggest very tentatively that the regions associated with a high

density of SFs may suffer a stronger droop than the regions without any SFs possibly due to In segregation. This might indicate that the SFs exacerbates the droop phenomenon in this zb SQW sample. This issue is worthy of further investigation.

Data availability statement

The data that support the findings of this study are openly available at the following URL/DOI: <https://doi.org/10.17863/CAM.101948>.

Acknowledgments

This work was enabled through financial support by Innovate UK through the Energy Catalyst Round 2—Early Stage Feasibility scheme (Ref. 132135): ‘To demonstrate the potential to make low cost, high efficiency LEDs using 3C-SiC substrates’, and by EPSRC through platform Grant No. EP/M010589/1: ‘Beyond Blue: New Horizons in Nitrides’ and research Grant No. EP/R01146X/1: ‘Fundamental studies of zincblende nitride structures for optoelectronic applications’. D J Wallis would like to thank the support of EPSRC through Grant No. EP/N01202X/2. The CL facility was funded by EPSRC under EP/R025193/1.

ORCID iDs

Abhiram Gundimeda  <https://orcid.org/0000-0001-5208-1920>

Gunnar Kusch  <https://orcid.org/0000-0003-2743-1022>

Rachel A Oliver  <https://orcid.org/0000-0003-0029-3993>

References

- [1] Zhou C, Ghods A, Saravade V G, Patel P V, Yunghans K L, Ferguson C, Feng Y, Kucukgok B, Lu N and Ferguson I T 2017 Review—the current and emerging applications of the III-nitrides *ECS J. Solid State Sci. Technol.* **6** Q149
- [2] Wu Y *et al* 2022 III-nitride nanostructures: emerging applications for Micro-LEDs, ultraviolet photonics, quantum optoelectronics, and artificial photosynthesis *Prog. Quantum Electron.* **85** 100401
- [3] Herrnsdorf J *et al* 2015 Active-matrix GaN micro light-emitting diode display with unprecedented brightness *IEEE Trans. Electron Devices* **62** 1918
- [4] Zissis G, Bertoldi P and Serrenho T 2021 Update on the status of LED-lighting world market since 2018 *EUR 30500 EN* (Publications Office of the European Union) (<https://doi.org/10.2760/759859>)
- [5] Schubert E F and Kim J K 2005 Solid-state light sources getting smart *Science* **308** 1274–8
- [6] Lim S-H, Ko Y-H, Rodriguez C, Gong S-H and Cho Y-H 2016 Electrically driven, phosphor-free, white light-emitting diodes using gallium nitride-based double concentric truncated pyramid structures *Light Sci. Appl.* **5** e16030
- [7] Auf Der Maur M, Pecchia A, Penazzi G, Rodrigues W and Di Carlo A 2016 Efficiency drop in green InGaN/GaN light emitting diodes: the role of random alloy fluctuations *Phys. Rev. Lett.* **116** 027401
- [8] Ren C X 2016 Polarisation fields in III-nitrides: effects and control *Mater. Sci. Technol.* **32** 418

- [9] Oliver R A 2016 Critical assessment 23: gallium nitride-based visible light-emitting diodes *Mater. Sci. Technol.* **32** 737
- [10] Zhao X, Sun K, Cui S, Tang B, Hu H and Zhou S 2023 Recent progress in long-wavelength InGaN light-emitting diodes from the perspective of epitaxial structure *Adv. Photon. Res.* **4** 2300061
- [11] Massabuau F C-P *et al* 2014 The impact of trench defects in InGaN/GaN light emitting diodes and implications for the 'green gap' problem *Appl. Phys. Lett.* **105** 112110
- [12] Armstrong A M, Crawford M H and Koleske D D 2014 Contribution of deep-level defects to decreasing radiative efficiency of InGaN/GaN quantum wells with increasing emission wavelength *Appl. Phys. Express* **7** 032101
- [13] Langer T, Jönen H, Kruse A, Bremers H, Rossow U and Hangleiter A 2013 Strain-induced defects as nonradiative recombination centers in green-emitting GaInN/GaN quantum well structures *Appl. Phys. Lett.* **103** 022108
- [14] Zhu M, You S, Detchprohm T, Paskova T, Preble E A, Hanser D and Wetzel C 2010 Inclined dislocation-pair relaxation mechanism in homoepitaxial green GaInN/GaN light-emitting diodes *Phys. Rev. B* **81** 125325
- [15] Hanada T 2009 Basic properties of ZnO, GaN, and related materials *Oxide and Nitride Semiconductors: Processing, Properties, and Applications* ed T Yao and S K Hong (Springer) p 1
- [16] Lee L Y, Frentrup M, Vacek P, Kappers M J, Wallis D J and Oliver R A 2019 Investigation of stacking faults in MOVPE-grown zincblende GaN by XRD and TEM *J. Appl. Phys.* **125** 105303
- [17] Lee L Y, Frentrup M, Kappers M J, Oliver R A, Humphreys C J and Wallis D J 2018 Effect of growth temperature and V/III-ratio on the surface morphology of MOVPE-grown cubic zincblende GaN *J. Appl. Phys.* **124** 105302
- [18] Gundimeda A, Rostami M, Frentrup M, Hinz A, Kappers M J, Wallis D J and Oliver R A 2022 Influence of Al_xGa_{1-x}N nucleation layers on MOVPE-grown zincblende GaN epilayers on 3C-SiC/Si(001) *J. Phys. D: Appl. Phys.* **55** 175110
- [19] Wade T J, Gundimeda A, Kappers M J, Frentrup M, Fairclough S M, Wallis D J and Oliver R A 2023 MOVPE studies of zincblende GaN on 3C-SiC/Si(0 0 1) *J. Cryst. Growth* **611** 127182
- [20] Kemper R M, Veit P, Mietze C, Dempewolf A, Wecker T, Bertram F, Christen J, Lindner J K N and As D J 2015 STEM-CL investigations on the influence of stacking faults on the optical emission of cubic GaN epilayers and cubic GaN/AlN multi-quantum wells *Phys. Status Solidi c* **12** 469
- [21] Lorenz K, Gonsalves M, Kim W, Narayanan V and Mahajan S 2000 Comparative study of GaN and AlN nucleation layers and their role in growth of GaN on sapphire by metalorganic chemical vapor deposition *Appl. Phys. Lett.* **77** 3391
- [22] Wei C H, Xie Z Y, Li L Y, Yu Q M and Edgar J H 2000 MOCVD growth of cubic GaN on 3C-SiC deposited on Si(100) substrates *J. Electron. Mater.* **29** 317
- [23] Ding B, Frentrup M, Fairclough S M, Kusch G, Kappers M J, Wallis D J and Oliver R A 2021 Multimicroscopy of cross-section zincblende GaN LED heterostructure *J. Appl. Phys.* **130** 115705
- [24] Ding B, Frentrup M, Fairclough S M, Kappers M J, Jain M, Kovács A, Wallis D J and Oliver R A 2020 Alloy segregation at stacking faults in zincblende GaN heterostructures *J. Appl. Phys.* **128** 145703
- [25] OSRAM (available at: www.mouser.co.uk/new/ams-osram/osram-oslon-square-gd-csbrm214-deep-blue-led/)
- [26] Verzellesi G, Saguatti D, Meneghini M, Bertazzi F, Goano M, Meneghesso G and Zanoni E 2013 Efficiency droop in InGaN/GaN blue light-emitting diodes: physical mechanisms and remedies *J. Appl. Phys.* **114** 71101
- [27] Tsai Y-C, Leburton J-P and Bayram C 2022 Quenching of the efficiency droop in cubic phase InGaAlN light-emitting diodes *IEEE Trans. Electron Devices* **69** 3240
- [28] Oliver R A *et al* 2013 The impact of gross well width fluctuations on the efficiency of GaN-based light emitting diodes *Appl. Phys. Lett.* **103** 141114
- [29] Drouin D, Couture A R, Joly D, Tastet X, Aimez V and Gauvin R 2007 CASINO V2.42—A fast and easy-to-use modeling tool for scanning electron microscopy and microanalysis users *Scanning* **29** 92
- [30] Cameron D, Edwards P R, Mehnke F, Kusch G, Sulmoni L, Schilling M, Wernicke T, Kneissl M and Martin R W 2022 The influence of threading dislocations propagating through an AlGaIn UVC LED *Appl. Phys. Lett.* **120** 162101
- [31] Church S A *et al* 2018 Effect of stacking faults on the photoluminescence spectrum of zincblende GaN *J. Appl. Phys.* **123** 185705
- [32] Shabunina E, Averkiev N, Chernyakov A, Levinshtein M, Petrov P and Shmidt N 2013 Extended defect system as a main source of non-radiative recombination in InGaN/GaN LEDs *Phys. Status Solidi C* **10** 335
- [33] Petroff P M and Lang D V 1977 A new spectroscopic technique for imaging the spatial distribution of nonradiative defects in a scanning transmission electron microscope *Appl. Phys. Lett.* **31** 60–62
- [34] Pennycook S J, Brown L M and Craven A J 1980 Observation of cathodoluminescence at single dislocations by STEM *Phil. Mag. A* **41** 589–600
- [35] Loeto K, Kusch G, Coulon P-M, Fairclough S M, Boulbar E L, Gírgel I, Shields P A and Oliver R A 2021 Point defects in InGaN/GaN core-shell nanorods: role of the regrowth interface *Nano Express* **2** 014005
- [36] Kusch G, Frentrup M, Hu N, Amano H, Oliver R A and Pristovsek M 2022 Defect characterization of 10–13 GaN by electron microscopy *J. Appl. Phys.* **131** 35705
- [37] Sugahara T, Sato H, Hao M, Naoi Y, Kurai S, Tottori S, Yamashita K, Nishino K, Romano L T and Sakai S 1998 Direct evidence that dislocations are non-radiative recombination centers in GaN *Jpn. J. Appl. Phys.* **37** L398
- [38] Weatherley T F K, Liu W, Osokin V, Alexander D T L, Taylor R A, Carlin J-F, Butté R and Grandjean N 2021 Imaging nonradiative point defects buried in quantum wells using cathodoluminescence *Nano Lett.* **21** 5217–24
- [39] Barthel A, Sayre L, Kusch G, Oliver R A and Hirst L C 2022 Radiation effects in ultra-thin GaAs solar cells *J. Appl. Phys.* **132** 184501
- [40] Church S A, Quinn M, Cooley-Greene K, Ding B, Gundimeda A, Kappers M J, Frentrup M, Wallis D J, Oliver R A and Binks D J 2021 Photoluminescence efficiency of zincblende InGaN/GaN quantum wells *J. Appl. Phys.* **129** 175702
- [41] Lähnemann J, Jahn U, Brandt O, Flissikowski T, Dogan P and Grahn H T 2014 Luminescence associated with stacking faults in GaN *J. Phys. D: Appl. Phys.* **47** 423001
- [42] Speck J S and Chichibu S F 2009 Nonpolar and semipolar group III nitride-based materials *MRS Bull.* **34** 304–12
- [43] Scholz F 2012 Semipolar GaN grown on foreign substrates: a review *Semicond. Sci. Technol.* **27** 24002
- [44] Bruckbauer J *et al* 2021 Influence of micro-patterning of the growth template on defect reduction and optical properties

- of non-polar (112 $\bar{0}$) GaN *J. Phys. D: Appl. Phys.* **54** 025107
- [45] Yeh C-Y, Wei S-H and Zunger A 1994 Relationships between the band gaps of the zinc-blende and wurtzite modifications of semiconductors *Phys. Rev. B* **50** 2715–8
- [46] Majewski J A and Vogl P 1998 Polarization and band offsets of stacking faults in AlN and GaN *MRS Internet J. Nitride Semicond. Res.* **3** e21
- [47] Belabbes A, de Carvalho L C, Schleife A and Bechstedt F 2011 Cubic inclusions in hexagonal AlN, GaN, and InN: electronic states *Phys. Rev. B* **84** 125108
- [48] Murayama M and Nakayama T 1994 Chemical trend of band offsets at wurtzite/zinc-blende heterocrystalline semiconductor interfaces *Phys. Rev. B* **49** 4710–24
- [49] Rebane Y T, Shreter Y G and Albrecht M 1997 Stacking faults as quantum wells for excitons in wurtzite GaN *Phys. Status Solidi a* **164** 141–4
- [50] Stampfl C and Van de Walle C G 1998 Energetics and electronic structure of stacking faults in AlN, GaN, and InN *Phys. Rev. B* **57** R15052–5
- [51] Takeuchi T, Sota S, Katsuragawa M, Komori M, Takeuchi H, Hiroshi Amano H A and Isamu Akasaki I A 1997 Quantum-confined stark effect due to piezoelectric fields in GaInN strained quantum wells *Jpn. J. Appl. Phys.* **36** L382
- [52] Dawson P, Schulz S, Oliver R A, Kappers M J and Humphreys C J 2016 The nature of carrier localisation in polar and nonpolar InGaN/GaN quantum wells *J. Appl. Phys.* **119** 181505